Near-field Raman imaging of organic molecules by an apertureless metallic probe scanning optical microscope

Norikiko Hayazawa[a)]
Department of Applied Physics, Osaka University, Suita, Osaka 565-0871, Japan, and CREST, Japan Corporation of Science and Technology, Japan

Yasushi Inouye
CREST, Japan Corporation of Science and Technology, Japan, Handai FRC, Suita, Osaka 565-0871, Japan, and School of Frontier Bioscience, Osaka University, Suita, Osaka 565-0871, Japan

Zouheir Sekkat
Department of Applied Physics, Osaka University, Suita, Osaka 565-0871, Japan, CREST, Japan Corporation of Science and Technology, Japan, Handai FRC, Suita, Osaka 565-0871, Japan, and School of Science and Engineering, Al Akhawayn University in Ifrane, 53000 Ifrane, Morocco

Satoshi Kawata
Department of Applied Physics, Osaka University, Suita, Osaka 565-0871, Japan, CREST, Japan Corporation of Science and Technology, Japan, Handai FRC, Suita, Osaka 565-0871, Japan, and RIKEN, Wako, Saitama, 351-0198, Japan

(Received 25 February 2002; accepted 23 April 2002)

Near-field Raman imaging of organic molecules is demonstrated by an apertureless near-field scanning optical microscope, the tip of which is a silver-layer-coated cantilever of an atomic force microscope (AFM). The virtue of the enhanced electric field at the tip apex due to the surface plasmon polariton excitations enhances the Raman scattering cross sections. This phenomenon allows us to reveal from near-field Raman images the molecular vibrational distributions of Rhodamine6G and Crystal Violet molecules beyond the diffraction limit of a light. These molecular vibrations cannot be distinguished by AFM topographic images. © *2002 American Institute of Physics.* [DOI: 10.1063/1.1485731]

I. INTRODUCTION

Near-field spectroscopy, such as fluorescence, infrared absorption, and Raman scattering, is a very powerful tool for the *in situ* chemical analysis of organic molecules in nanometer scale. Raman scattering and infrared absorption spectroscopy allow the direct observation of molecular vibrations without necessarily photobleaching of the sample as well as quenching. While conventional Raman spectroscopy is relatively straightforward to carry out with well-established light sources and instruments in the visible region, the Raman scattering cross sections ($\sim 10^{-30}\,\mathrm{cm}^2$) are much smaller than that of fluorescence ($\sim 10^{-16}\,\mathrm{cm}^2$) and infrared absorption ($\sim 10^{-20}\,\mathrm{cm}^2$). Moreover, in a near-field scanning optical microscope (NSOM) setup, the observed volume of the sample must be confined in the nanometer scale that corresponds to the very small size of molecules. These make it difficult to realize near-field Raman spectroscopy. Jahncke *et al.* first reported near-field Raman imaging by using a NSOM with an optical fiber probe (aperture probe),[1] however, due to the long integration time caused by the very small Raman scattering cross section and the low throughput of aperture probes, image acquisition took more than 10 h to complete one near-field Raman image of the 4 $\mu\mathrm{m}^2$ region. To circumvent this problem, the use of an apertureless metallic probe tip[2–4] provides an enhanced electric field at the tip apex due to the surface plasmon polariton excitations.[5–8] Furthermore, near-field Raman spectroscopy using this technique could have higher resolution since a smaller tip size can be attainable due to the ''lightening rod effect.''[8] In recent works, the enhanced electric field at the metallic tip has been successfully applied to near-field single photon fluorescence,[9–13] two-photon fluorescence excitation spectroscopy,[14] and near-field surface-enhanced infrared absorption spectroscopy.[15,16] On the other hand, near-field Raman spectroscopy that utilizes electromagnetic field enhancement at the metallic tip has been proven to achieve chemical analysis of organic materials by mapping the near-field Raman spectra at several positions in a nanometer scale.[17–20] In our recent work,[18,20] we have measured the near-field Raman spectra of dye molecules with a spatial resolution within the nanometer range that enabled us to assign Stokes-shifted lines to each vibration mode of each molecule. It was also observed to have an enhanced Raman intensity and shift of specific Stokes-shifted lines that was induced by chemical interaction between the metallic tip and Raman active molecules.[20–22] In another work, intensity enhancement of all Stokes-shifted lines induced by the locally enhanced electric field at the metallic tip was also observed.[18] In contrast to the NSOM utilizing an aperture probe, the strong enhancement phenomena drastically reduce

[a)]Author to whom correspondence should be addressed. Electronic mail: hayazawa@ap.eng.osaka-u.ac.jp Phone: +81-6-6879-7847; fax: +81-6-6879-7330.

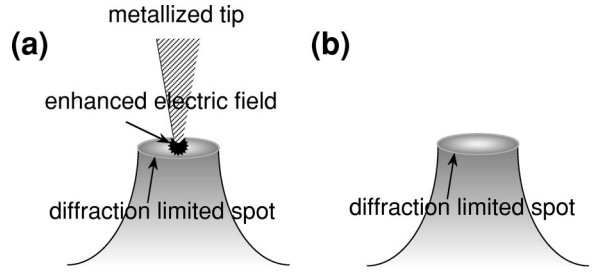

FIG. 1. The conceptual figure of (a) near-field Raman detection by a metallic probe tip as compared to (b) normal micro-Raman detection (farfield detection).

the measurement time when using a NSOM with a metallic apertureless tip (*vide infra*). In our previous experiment,[18,20] it took only 1 s to obtain a near-field Raman spectrum using a spectrophotometer equipped with a liquid-nitrogen-cooled CCD camera. The short acquisition time that is due to the strong enhancement at the metallic tip enabled us to obtain near-field Raman imaging within a reasonable time (~10 min). The near-field Raman imaging can attain direct and sensitive observation of many kinds of molecules and their local distributions, as well as biological cells without labeling with dye. In this paper, we demonstrate two-dimensional near-field Raman imaging at specific Stokes-shifted lines of aggregates of nanocrystallized Rhodamine6G and Crystal Violet molecules by using a silver-coated cantilever tip. We achieved 10 minutes data-acquisition time for each near-field Raman image of 1 μm by 1 μm consisting of the 64 pixels by 64 pixels image.

II. EXPERIMENTAL SECTION

Figure 1 shows the concept of (a) near-field Raman spectroscopy as compared to (b) micro-Raman spectroscopy (farfield detection). In Fig. 1(a), the Raman scattering cross sections of the molecules just below the enhanced electric field at the metallic tip are selectively enhanced and detected to provide a sufficiently high spatial resolution depending on the size of the enhanced electric field that corresponds to the diameter of the metallic tip, e.g., less than 40 nm.[5–8]

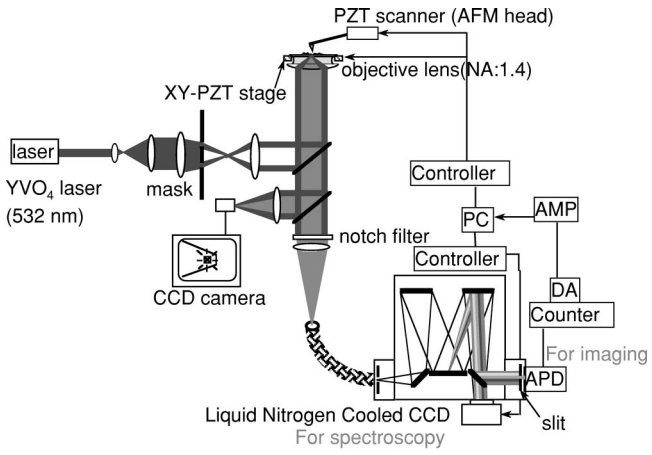

FIG. 2. Experimental setup for near-field Raman imaging.

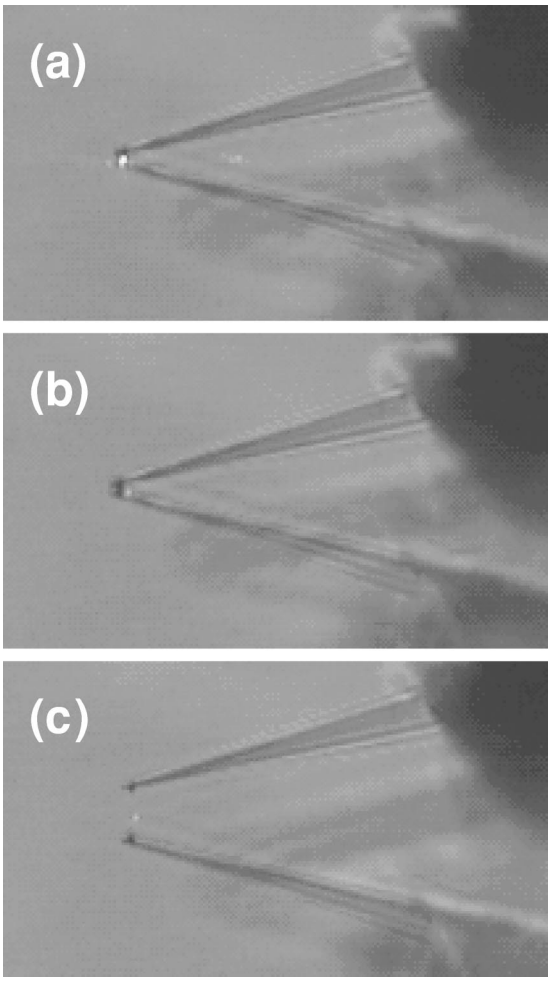

FIG. 3. The CCD images of the scattering of the evanescent field at the metallic tip observed when the distance between the probe and sample surface of the focused spot are (a) 0 nm (in contact), (b) 50 nm, and (c) 30 μm. Each image shows the cantilever and its mirror image on the sample surface. The bright spot at the tip in (a) is the scattering of the evanescent field, whereas the weak light spots at the sample surface in (b) and (c) are the Rayleigh scattering at the focused spot due to the sample roughness.

The experimental setup for the near-field Raman imaging is shown in Fig. 2. An expanded and collimated light field from a frequency doubled YVO_4 laser (wavelength: 532 nm; power: 50 mW) enters into the epi-illumination optics. A circular mask is inserted in the beam path of the illumination light and located at the conjugate plane of the pupil of the objective lens with numerical aperture (NA) equal to 1.4. The mask rejects the part of the beam corresponding to focusing angles that are less than NA=1.0 while the transmitted light forms a focused spot that produces an evanescent field on the sample surface.[9] As the distance of the metallic tip is moved closer to the focused spot, a localized enhanced electric field is observed to be generated at the tip apex.[5–7] Figure 3 shows the CCD images of the scattering of the evanescent field at the metallic tip observed from the side of the metallic tip. Figure 3(a) is obtained when the tip is in contact with the sample surface of the focused spot. Figures 3(b) and 3(c) are obtained when the distance between the tip and the sample surface are 500 nm and 30 μm, respectively. Figure 3(a) exhibits the very bright scattering light of the evanescent field from the tip apex. Consequently, the highly

p-polarized evanescent field excites surface plasmon polaritons at the tip apex, and the enhanced electric field that is localized at the tip is generated in the case of Fig. 3(a), even though the enhanced electric field itself cannot be seen in the image since it is localized at the tip apex. However, in Figs. 3(b) and 3(c), no scattering of the evanescent field is observed because the tip is out of the skin depth of the evanescent field, and, thus, only very weak Rayleigh scattering light at the focused spot is observed due to the sample roughness. The localized enhanced electric field at the tip is scattered inelastically by the Raman active molecules, which corresponds to near-field Raman scattering. The Raman scattering is collected by the same objective lens, and is directed to the spectrophotometer (focal length=300 mm, 1200 lines/mm) that is equipped with a liquid-nitrogen-cooled CCD camera (1340×400 channels) for Raman spectra measurement and with an avalanche photodiode for Raman imaging. The avalanche photodiode is located after the exit slit of the spectrophotometer so that a specific Stokes-shifted line can be detected. Excitation light or Rayleigh scattering is sufficiently rejected by a notch filter (wavelength: 532 nm; full width at half-maximum: 6 nm). The metallic tip is a silicon cantilever that is coated by a 40 nm thick silver layer by a thermal evaporation process. The evaporation rate was adjusted to a relatively slow rate of 0.3 Å per second to avoid undesirable bending of the silicon tip. The silver-coated tip diameter is around 40 nm. The distance between the sample and the cantilever is regulated by contact-mode AFM operation, and the sample is scanned with piezoelectric transducers (PZT) in the $X-Y$ plane. Scanning the XY-PZT sample stage while simultaneously detecting the Raman signal with the avalanche photodiode can perform near-field Raman imaging at the specific Stokes-shifted line.

III. RESULTS AND DISCUSSION

Aggregates of Rhodamine6G and Crystal Violet molecules were used as samples for near-field Raman spectroscopy and imaging. Two separate samples are prepared by casting the ethanol solution of Rhodamine6G and Crystal Violet, both with 1.25×10^{-2} wt.% concentration. The samples are dried on a coverslip covered with an 8 nm thick silver film. The distribution of molecules for both samples is fairly inhomogeneous and is set to have a 1 nm average thickness of the layer of molecules. The silver film is one of the very popular surface enhancers of the surface-enhanced Raman scattering (SERS) effect,[8] and is effective not only in enhancement of a Raman scattering cross section, but also in the reduction of the fluorescence due to the fluorescence energy transfer from the molecules to metal.[23,24] Because both Rhodamine 6G and Crystal Violet have absorption at the excitation wavelength of 532 nm, and have fluorescence overlapped with Raman peaks. Consequently, the observed Raman spectra are due to surface-enhanced resonant Raman scattering (SERRS).[17,18,20] Figure 4 shows the Raman spectra of Rhodamine6G molecules, which was obtained (a) in the presence of the metallic tip that is in contact with the sample surface of the focused spot, and (b) without the tip. The Raman scattering spectrum of (a) comprises of the contribution of both the locally enhanced electric field at the tip apex and the focused spot [see Fig. 1(a)], whereas the Raman scattering spectrum of (b) is due solely to the Raman scattering of the focused spot [see Fig. 1(b)]. The difference between the spectra (a) and (b) is the inherent near-field Raman scattering induced by the metallic tip.[18,20] Several Stokes-shifted lines of Rhodamine6G molecules are observed and indicated by arrows in the spectra. These peaks are in good agreement with the former works by other authors.[24,25] For example, the peaks at 1359, 1503, 1570, and 1647 cm^{-1} are assigned to the C–C stretching vibration mode of the aromatic ring; the peak at 1269 cm^{-1} is assigned to the C–O–C (ester bonding) vibration mode; the peak at 1120 cm^{-1} is assigned to the C–H in-plane bending vibration mode; the peak at 766 cm^{-1} is assigned to the C–H out-of-plane bending vibration mode, and the peak at 607 cm^{-1} is assigned to the C–C–C in-plane bending vibration mode. The exposure time of the liquid-nitrogen-cooled CCD camera was 1 s and the power of the laser at the entrance of the inverted microscope was 230 μW.

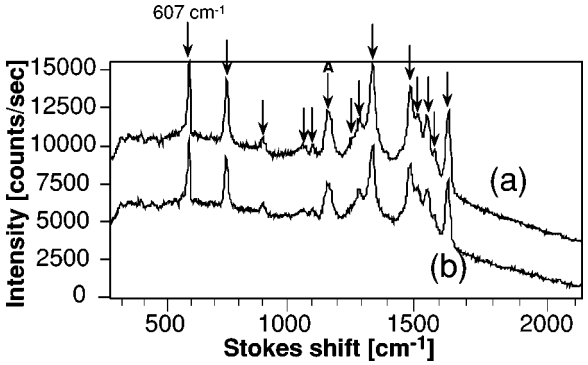

FIG. 4. Raman spectra of Rhodamine6G (a) with and (b) without a metallic tip. Arrows indicate the Raman peaks of Rhodamine6G molecules. The concentration of the molecules is 1.25×10^{-2} wt.%. Laser power: 230 μW, exposure time: 1 s. The peak at 607 cm^{-1} corresponding to the C–C–C in-plane bending vibration mode is used for near-field Raman imaging in Fig. 6(a). The peak at "A" (1185 cm^{-1}) of Rhodamine6G is slightly overlapped with the peak at 1172 cm^{-1} of Crystal Violet in Fig. 5, which is used for near-Raman imaging in Fig. 6(c).

Figure 5 shows the Raman spectra of Crystal Violet molecules. Spectra (a) and (b) have been obtained with and without the metallic tip, respectively. Raman scattering intensity of Crystal Violet is weaker than that of Rhodamine6G, however, several characteristic Stokes-shifted lines are observed. The peaks at 1383, 1537, 1586, and 1617 cm^{-1} are assigned to the C–C stretching vibration mode of the aromatic ring; the peak at 1363 cm^{-1} is assigned to the *N*-phenyl vibration mode; the peak at 1172 cm^{-1} is assigned to the C–H in-plane bending vibration mode; the peaks at 908 and 798 cm^{-1} are assigned to the C–H out-of-plane bending vibration mode, the peak at 414 cm^{-1} is assigned to the C–C–C out-of-plane bending vibration mode; and the peak at 332 cm^{-1} is assigned to the phenyl–C–phenyl vibration mode. These peaks correspond well with the results of other authors.[26–28] The peak at 2050 cm^{-1} is a ghost line, which came from the laser diode that was used as feedback in AFM operation.[29] The exposure time of the liquid-nitrogen-cooled CCD camera was 1 s with 230 μW laser power at the entrance of the inverted microscope.

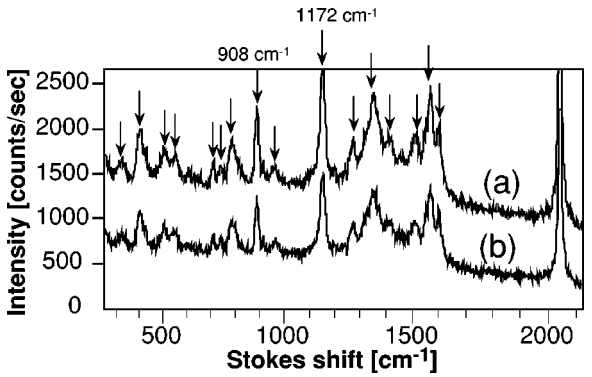

FIG. 5. Raman spectra of Crystal Violet (a) with and (b) without a metallic tip. Arrows indicate the Raman peaks of Crystal Violet molecules. The concentration of the molecules is 1.25×10^{-2} wt.%. Laser power: 230 μW, exposure time: 1 s. The peaks at 908 cm^{-1} corresponding to the C–H out-of-plane bending vibration mode and 1172 cm^{-1} corresponding to the C–H in-plane bending vibration mode are used for near-field Raman imaging in Figs. 6(b) and 6(c), respectively.

The enhancement factor of 100 due to the silver tip is obtained experimentally by defining the factor F as the ratio of the intensity of the near-field scattering to that of farfield intensity per unit area as

$$F=\frac{dI_n}{dI_f}, \tag{1}$$

where dI_n and dI_f are the Raman intensity per unit area in the near-field and farfield, respectively. Experimentally, we can get the intensity enhancement ratio as

$$\frac{I_n+I_f}{I_f}=\frac{dI_n^*\phi_n+dI_f^*\,\phi_f}{dI_f^*\,\phi_f}, \tag{2}$$

where I_n and I_f are the totally observed Raman intensity in the near-field and farfield, respectively. ϕ_n and ϕ_f are the near-field and farfield excitation light spot. Accordingly, I_n+I_f and I_f correspond to the Raman intensity with [Fig. 1(a)] and without [Fig. 1(b)] a metallic tip, respectively. From Figs. 4 and 5, I_n+I_f/I_f is approximately 2. Near-field excitation light spot ϕ_n is approximately the 40 nm diameter corresponding to the tip diameter[5–7] and the farfield excitation spot ϕ_f is approximately a 400 nm diameter that is focused by the objective lens with NA=1.4. By substituting these values to Eq. (2), we can obtain the enhancement factor $F=100$. The effect of near-field enhancement is proven by this high enhancement factor. The mirror effect of the cantilever tip (farfield effect), on the other hand, has an expected enhancement factor of $F\leqslant2$, and could not be the source of the high enhancement factor.

To investigate the spatial resolving power by our proposed near-field Raman spectroscopy and identify molecular vibration distribution among different kinds of molecules, near-field Raman images of an aggregated sample of Rhodamine6G and Crystal Violet molecules were obtained at characteristic Raman peaks of each molecules. Figure 6 shows near-field Raman images at the same area of the sample, where the concentrations of Rhodamine6G and Crystal Violet are 1.25×10^{-3} and 1.25×10^{-2} wt.%, respectively. These concentrations resulted in the comparable Raman scattering intensity from Rhodamine6G and Crystal Violet because Rhodamine6G yields a much higher scattering intensity than that of Crystal Violet molecules, as observed in the spectra of Figs. 4 and 5. Figure 6(a) is obtained at 607 cm^{-1}, which corresponds to the Stokes-shifted line of the C–C–C in-plane bending vibration mode of Rhodamine6G. Figure 6(b) is obtained at 908 cm^{-1}, which corresponds to the Stokes-shifted line of the C–H out-of-plane bending vibration mode of Crystal Violet and Fig. 6(c) is obtained at 1172 cm^{-1}, which corresponds to the Stokes-shifted line of the C–H in-plane bending vibration mode of Crystal Violet. Figure 6(d) is a corresponding topographic image obtained simultaneously with Fig. 6(a) in AFM operation. It is interesting to note that all the other Stokes-shifted lines except the ones used for the imaging are quite overlapped between Rhodamine6G and Crystal Violet. Also, the peak at 1172 cm^{-1} used for near-field Raman imaging in Fig.

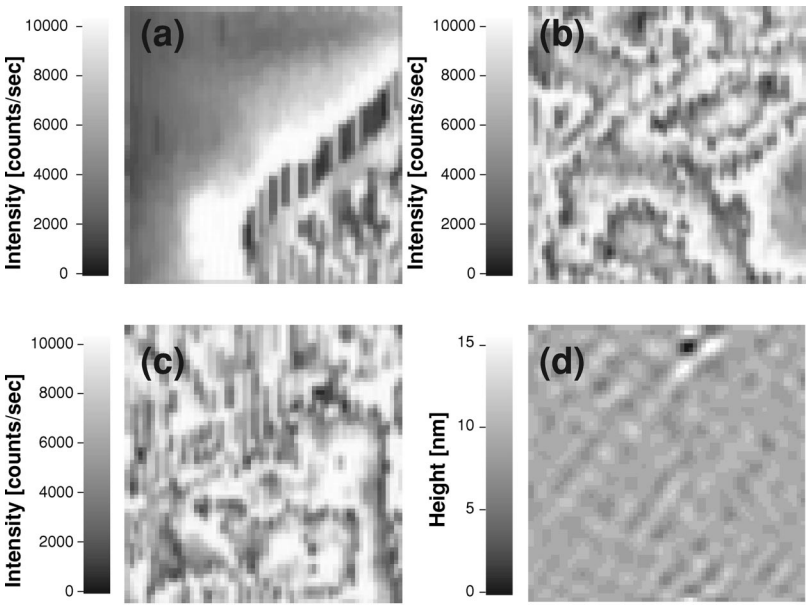

FIG. 6. (a) Near-field Raman images obtained at (a) 607 cm^{-1}; C–C–C in-plane bending mode of Rhodamine6G, (b) 908 cm^{-1}; C–H out-of-plane bending mode of Crystal Violet, and (c) 1172 cm^{-1}; C–H in-plane bending mode of Crystal Violet. (d) is the corresponding topographic image. It took 10 min to obtain one image where a 1 μm by 1 μm scanning area consisted of 64 by 64 pixels.

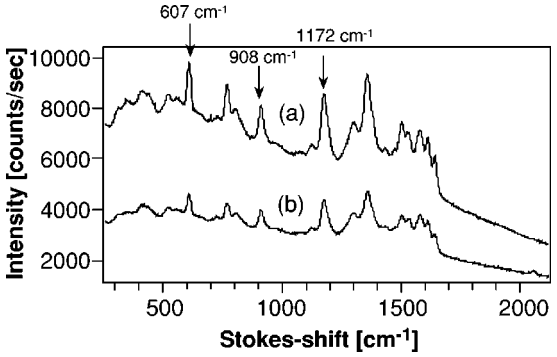

FIG. 7. Typical Raman spectra of the aggregated sample used in Fig. 6, (a) with and (b) without a metallic tip. Stokes-shifted lines of Rhodamine6G and Crystal Violet are observed. Arrows indicate the Stokes-shifted lines used for near-field Raman imaging in Fig. 6.

6(c) is slightly overlapped with the Stokes-shifted line of Rhodamine6G at 1185 cm^{-1}, which is indicated by alphabet ''A'' in Fig. 4. The dimension of both images with 64 pixels by 64 pixels resolution is 1 μm by 1 μm. The scanning rate used for each line is 0.1 Hz. At this rate, a single image can be achieved for only 10 min. Figure 7 shows the typical Raman spectra of the aggregated sample, which exhibits the Stokes-shifted lines of both Rhodamine6G and Crystal Violet molecules. The arrows in Fig. 7 point to the Stokes-shifted lines used for the near-field Raman imaging in Fig. 6. We can selectively obtain the distributions of each vibration mode that we cannot distinguish in the topographic image. The distributions of each vibration mode are quite different, and shows complicated structures corresponding to the inhomogeneous distributions of both molecules. According to Fig. 6(a), Rhodamine6G molecules are mainly localized at the lower right of the figure, on the other hand, Fig. 6(b) shows that Crystal Violet molecules are randomly dispersed in the scanned area. Interestingly, we can clearly see the different distributions between C–H out-of-plane bending [Fig. 6(b)] and C–H in-plane bending [Fig. 6(c)] of Crystal Violet molecules. The almost absence of Rhodamine6G molecules at the upper left of the scanned area in Fig. 6(a) can possibly explain the nonoverlap of the Stokes-shifted line at 1185 cm^{-1} of Rhodamine6G with the Stokes-shifted line at 1172 cm^{-1} of Crystal Violet. At this time, we do not have clear explanations for this phenomenon, however, we believe that this could be explained by the molecule–tip ''chemical'' interaction.[20–22] In our previous report,[20] we observed the selective enhancement and the shifts of some Stokes-shifted lines of Rhodamine6G molecules due to the chemical interaction between the tip and molecules. For example, C–H in-plane bending of Rhodamine6G at 1120 cm^{-1}, which is usually very weak compared to other Stokes-shifted lines, was strongly enhanced and shifted, on the other hand, C–H out-of-plane bending at 766 cm^{-1} was not chemically enhanced. Similarly, the Stokes-shifted line at 1185 cm^{-1} of Rhodamine6G was chemically enhanced (see Fig. 4 in Ref. 18). These strong chemical enhancement and shifts might have an affect in the near-field Raman image obtained at C–H in-plane bending of Crystal Violet at 1172 cm^{-1} in Fig. 6(c). So far, we have never observed such chemical enhancement of Crystal Violet molecules. The enhancement effect at the tip is somewhat very sensitive to the tip. In our experimental conditions, a few of ten probes coated with a silver layer exhibit the electric field enhancement effect at the tip. In the case of electric field enhancement, all the Raman peaks are similarly enhanced, and do not show band specific enhancement.[18] Furthermore, a few tens of probes that exhibit the electric field enhancement effect show the chemical enhancement.[19–22] So, the reproducibility is not so high as of now, however, once the probe showed either electric field or chemical enhancement, the enhancement effect is reproducible until the tip is broken mostly by the high roughness of the sample or dust stuck to the sample surface. In Fig. 6(d), the island structures of the silver film are observed in the topographic image because the average thickness of the aggregated molecular layer is estimated at 1 nm and much thinner than the silver film (average thickness: 8 nm). Accordingly, the distributions of both molecules are not clearly seen in the topographic image that reflects the pancake structure of the silver grains (30–50 nm in diameter and 8 nm in thickness). Note that without a metallic tip (farfield detection), we could not obtain such high-resolution images because the farfield signal is averaged inside of the focused spot [Fig. 1(b)].[30] Figure 6 shows that the near-field Raman images attain the molecular vibrational distributions with a high sensitivity, even if the thickness of the molecular layer is 1 nm. And, the sensitivity is approximately calculated to be the number of molecules just below the enhanced electric field (ϕ: 40 nm) by a factor of 10^3.[31] However, in fact, the total intensity enhancement in Figs. 4, 5 is almost due to the increased white continuum signal, which are usually seen as a broad underlying background of the SERS signal;[24] thus, the actual Raman peaks in Figs. 4 and 5 increase not by a factor of 2 but by 25%–35%. On the other hand, in Fig. 7, the Raman peaks in the mixed samples show somewhat larger enhancement by a factor of up to 2. These different enhancement factors may be attributed to the different probes used for Figs. 4, 5 and Figs. 6, 7. In this paper, we used organic dye molecules adsorbed on silver films. While the silver films are necessary for dye molecules to quench the strong fluorescence, near-field Raman spectroscopy, and imaging by an apertureless metallic probe scanning optical microscope is applicable, not only to an organic sample but also to an inorganic sample, even without the support of the silver films. Single molecule detection can be done after idealizing the tip material, shape,[14] and illumination method[6] because the enhancement factor is very sensitive to the tip and the polarization of the light.

We have demonstrated the near-field Raman imaging by using the highly localized enhancement virtue of a metallic tip apertureless NSOM. Raman images of Raman active molecules have been obtained at very high spatial resolutions and with 10 min data-acquisition time. Near-field Raman imaging with a metallic tip will allow for single molecule detections and imaging of various kinds of molecules, and in particular, nonfluorescent molecules.

ACKNOWLEDGMENT

This work was supported by a grant for Scientific Research from the Ministry of Education, Science, and Culture of Japan. We thank Dr. V. Daria and A. Tarun for their valuable comments and discussions on this work.

[1] C. L. Jahncke, M. A. Paesler, and H. D. Hallen, Appl. Phys. Lett. **67**, 2483 (1995).
[2] U. Ch. Fischer and D. W. Pohl, Phys. Rev. Lett. **62**, 458 (1989).
[3] Y. Inouye and S. Kawata, Opt. Lett. **19**, 159 (1994).
[4] R. Bachelot, P. Gleyzes, and A. C. Boccara, Opt. Lett. **20**, 1924 (1995).
[5] H. Furukawa and S. Kawata, Opt. Commun. **148**, 221 (1998).
[6] L. Novotny, E. J. Sanchez, and X. S. Xie, Ultramicroscopy **71**, 21 (1998).
[7] J. Jersch, F. Demming, L. J. Hildenhagen, and K. Dickmann, Appl. Phys. A: Mater. Sci. Process. **66**, 29 (1998).
[8] R. K. Chang and T. E. Furtak, *Surface Enhanced Raman Scattering* (Plenum, New York, 1982).
[9] N. Hayazawa, Y. Inouye, and S. Kawata, J. Microsc. **194**, 472 (1999).
[10] J. Azoulav, A. Debarre, A. Richard, and T. Tchenio, J. Microsc. **194**, 486 (1999).
[11] H. F. Hamann, A. Gallagher, and D. J. Nesbitt, Appl. Phys. Lett. **76**, 1953 (2000).
[12] T. J. Lessard, G. A. Lessard, and S. R. Quake, Appl. Phys. Lett. **76**, 378 (2000).
[13] H. F. Hamann, M. Kuno, A. Gallagher, and D. J. Nesbitt, J. Chem. Phys. **114**, 8596 (2001).
[14] E. J. Sanchez, L. Novotny, and X. S. Xie, Phys. Rev. Lett. **82**, 4014 (1999).
[15] A. Lahrech, R. Bachelot, P. Gleyzes, and A. C. Boccara, Appl. Phys. Lett. **71**, 575 (1997).
[16] B. Knoll and F. Keilmann, Nature (London) **399**, 134 (1999).
[17] Y. Inouye, N. Hayazawa, K. Hayashi, Z. Sekkat, and S. Kawata, Proc. SPIE **3791**, 40 (1999).
[18] N. Hayazawa, Y. Inouye, Z. Sekkat, and S. Kawata, Opt. Commun. **183**, 333 (2000).
[19] R. M. Stockle, Y. D. Suh, V. Deckert, and R. Zenobi, Chem. Phys. Lett. **318**, 131 (2000).
[20] N. Hayazawa, Y. Inouye, Z. Sekkat, and S. Kawata, Chem. Phys. Lett. **335**, 369 (2001).
[21] A. Otto, I. Mrozek, H. Grabhorn, and W. Akemann, J. Phys.: Condens. Matter **4**, 1143 (1992).
[22] P. Kambhampati and A. Campion, Surf. Sci. **427–428**, 115 (1999).
[23] R. R. Chance, A. Prock, and R. Silbey, Adv. Chem. Phys. **37**, 1 (1978).
[24] S. Nie and S. R. Emory, Science **275**, 1102 (1997).
[25] P. Hildebrandt and M. Stockburger, J. Phys. Chem. **88**, 5935 (1984).
[26] J. Gicquel, M. Carles, and H. Bodot, J. Phys. Chem. **83**, 699 (1979).
[27] S. Sunder and H. J. Bernstein, Can. J. Chem. **59**, 964 (1981).
[28] T. Watanabe and B. Pettingger, Chem. Phys. Lett. **89**, 501 (1982).
[29] Whether this ghost line appears or not is due to the position where the LD is focused on a cantilever.
[30] In the case of the mixed sample that we used for imaging, both Rhodamine6G and Crystal Violet molecules are randomly dispersed on the silver-coated cover slip so that the farfield Raman signal from the focused spot is averaged to an almost constant value.
[31] The actual density of the molecules were roughly estimated from the thickness of the sample compared with the well-known sample that we used in Ref. 18.